Charge storage characteristics and tunneling mechanism of amorphous Ge-doped HfO_x films

X.Y. Qiu[1)] *, S. Y. Zhang[1)], T. Zhang[1)], R. X. Wang[1)], L.T. Li[1)], Y. Zhang[1)], J. Y. Dai[2)]

[1)] *School of Physical Science and Technology, Southwest University, Chongqing 400715, China*

[2)] *Department of Applied Physics, the Hong Kong Polytechnic University, Hong Kong, China*

** Corresponding author's email: qxy2001@swu.edu.cn*

Abstract: Amorphous Ge-doped HfO_x films have been deposited on p-Si(100) substrates by means of RF magnetron sputtering. Microstructural investigations reveal the partial oxidation of doped Ge atoms in the amorphous HfO_x matrix and the existence of $HfSiO_x$ interfacial layer. Capacitance-voltage hysteresis of the Ag/ Ge-doped HfO_x /Si/Ag memory capacitor exhibits a memory window of 3.15 V which can maintain for more than 5×10^4 cycles. Current-voltage characteristics reveal that Poole–Frenkel tunneling is responsible for electron transport in the Ge-doped HfO_x film.

Key words: Ge-doped HfO_x film; charge storage characteristic; tunneling mechanism

1. Introduction

Flash memory devices store information in the charge state of a capacitor, and the presence or absence of charges represents logic "1" or "0". With the continuous scaling-down of flash memory devices, the high field stressing and the leaky scaled-down oxide barrier result in the disastrous leakage current problem. This promotes an intensive study on nano-floating-gate nonvolatile memories based on the field-effect transistor structure with isolated nano-particles embedded in the gate dielectrics[1]. Up to now, many oxide dielectric materials (SiO_2[2], HfO_2[3-6], Al_2O_3[7], $HfAlO_x$[8-10], $LaAlO_3$[11], Si_xGe_yO[12-13] etc.), semiconductor materials (GaAs[14], ZrO_2[15] etc.), graphene oxide[16], organic dielectrics[17-18], and hybrid halid perovskite [19] have been studied for potential candidates for tunneling/control oxides. HfO_2 is highlighted due to its high permittivity (20~30), large band gap (~ 6 eV) and good chemical stabilities on silicon [20-21]. On the other hand, various kinds of nano-particles (NPs), including metal (Ag[5,8], Au[9], Pt[14] etc.), semiconductor (Ge[2-4,10-12], Si[6], SiGe[15] etc.) and high-κ dielectric nano-particles (HfO_2[22], TiN[23] and CeO_2[24]) have been considered to be candidates for memory nano-dots. The above alternative materials give a flat band voltage shift $|\Delta V_{FB}|$ ranging from 1 to 12 V, a trapped charge density of 10^{11}-10^{13} electrons/cm^2 and an endurance

performance of 10^3-10^5 cycles. These memory structures possess the advantages in film thickness (< 10 nm) and small leakage current density (< 10^{-3}A/cm^2), however, their trapped charge density and endurance properties are still lower than that of current commercial metal-gate MNOS (Metal/Nitride/Oxide/Silicon) memory device (a charge density of 10^{18}-10^{19} electrons/cm^3 and a excellent endurance of 10^6-10^{10} cycles)

Ge is one of the attractive memory nano-dots candidates because of its small band gap (~ 0.6 eV) and large work function (~ 5 eV). Previous research reports [2-4,10-12] have revealed that Ge NPs embedded in various kinds of amorphous dielectric films (SiO_2, HfO_2, $LaAlO_3$ etc.) can give a memory window width ranging from 0.8 to 12 V, but its high crystalline temperature (> 600℃), poor endurance property(~10^3 cycles) and oxidization in oxide matrix are main obstacles for potential applications in next-generation flash memory devices. On the other hand, we notice that there are few reports on memory characteristics of amorphous Ge-doped HfO_x film. In fact, amorphous films are more beneficial to suppress leakage current than polycrystalline films due to the lack of grain boundary defects. In this paper, amorphous HfO_x film doped with amorphous Ge atoms is studied, and its microstructure, memory property and tunneling mechanism are investigated.

2. Experimental details

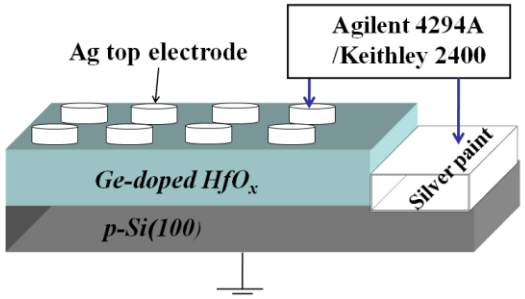

Figure 1 (color online) Schematic illustration of the capacitor structure based on Ge-doped HfO_x films

p-type Si (100) substrates were ultrasonically cleaned in acetone, then dipped in diluted hydrofluoric solution (4%) for 2 min to remove the native silicon oxide and leave a H-terminated surface. In 3 Pa Ar+O_2 ambient (Ar:O_2=30:10 SCCM), a 10 nm-thick Ge-doped HfO_x film was deposited at room temperature on the etched substrate by co-sputtering a HfO_2 target (99.99 % purity) covered by a quadrant Ge sheet (99.99 % purity) with a Ge/HfO_2 area ratio of 1:3. The working power of sputtering is 70 W. After annealing at 300℃ in N_2 atmosphere for 30 min, the film sample was covered by a shadow mask with 0.2 mm-diameter pinholes. Then,

100 nm-thick Ag top electrodes were deposited on the film sample at 200℃in 0.5 Pa Ar ambient by using direct current magnetron sputtering. After painting silver paint on the bare Si substrate to act as bottom electrode, a capacitor structure of Ag/Ge-doped HfO_x/Si/Ag as shown in fig.1 was obtained. In order to make a comparison, a reference sample of pure HfO_x film without Ge was also deposited and annealed under same conditions.

Microstructure of the sample was investigated by means of transmission electron microscopy (TEM, JEM-2100F), and film's chemical composition was investigated by means of x-ray photoelectron spectroscopy (XPS, ESCALAB 250) combined with Ar^+ etching technology. After applying the gate voltage to the top Ag electrodes and the silver paint while holding Si substrate at ground, capacitance-voltage (*C*-*V*) curves and endurance properties were measured using the Agilent 4294A impedance analyzer, and leakage current density-voltage (*J*-*V*) curves were measured using Keithley 2400 source meter.

3. Results and discussions

3.1 Microstructure of the Ge-doped HfO_x film

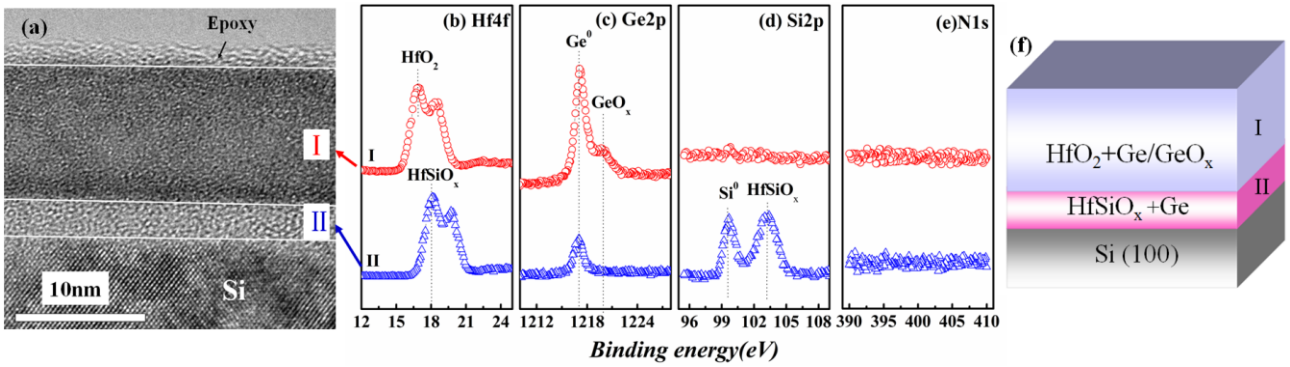

Figure 2 (color online) (a) Cross-section TEM image, XPS depth profile spectra of (b) Hf4f, (c) Ge2p, (d) Si2p and (e) N1s core levels, and (f) the composition illustration of the Ge-doped HfO_x film.

Table 1 Statistical analyses on elements in the Ge-doped HfO_x film

Elements / Etching Level	Hf4f (at %)	Ge2p (at %)	Si2p (at %)	O1s (at %)
Ⅰ (film)	22.49657	21.9367	0.41455	55.1522
Ⅱ (interfacial layer)	10.83891	10.8011	25.2634	53.0966

Figure 2a is a cross-section TEM image of the Ge-doped HfO_x film, where one can see that the 10 nm-thick HfO_x film is amorphous structure (Ⅰ) without crystallized Ge clusters. It is apparent, however, an unexpected 3 nm-thick amorphous interfacial layer (Ⅱ) is formed. The film's compositions are identified by means of XPS combined with Ar^+ etching technology. After cleaning the surface by pre-etching for 5 s, this sample was etched layer-by-layer from amorphous film (Ⅰ) to interfacial layer (Ⅱ). Typical charge-corrected XPS depth profile spectra are shown in figs.2b-2d. As shown in fig.2b, when the sample is etched from the amorphous film (Ⅰ) to the interfacial layer (II), the binding energy of Hf4f core level shifts from 16.3 eV (corresponding to Hf-O bond in HfO_2) to 18.1eV (corresponding to Hf-O bond in $HfSiO_x$). For Ge2p core level shown in fig.2c, a strong Ge^0 peak (~1217 eV) and a weak GeO_x peak (~1219 eV) are simultaneously observed in the film (Ⅰ), revealing that partial Ge atoms doped in the HfO_x matrix have been oxidized into GeO_x. After further etching to the interfacial layer (II), the GeO_x peak vanishes, and the Ge^0 peak becomes very weak. This implies that there are some Ge atoms present in the $HfSiO_x$ interfacial layer. Why Ge atoms in the interfacial layer is not oxidized? Possible reasons are: (1) both Si-O and Hf-O bonds have a lower Gibbs free energy than Ge-O bond [25]; (2) the standard Gibbs energy of formation for both HfO_2 (-1088.2 kJ/mol) and SiO_2 (-856.3 kJ/mol) are lower than that of GeO (-237.2 kJ/mol)[26]. This implies that oxygen ions are easier to bond with Si or Hf ions than Ge ions. In other words, oxygen-deficient $HfSiO_x$ in the interfacial layer will grab oxygen atoms from GeO_x, and reduce GeO_x to Ge atoms. For Si2p core level shown in fig.2d, Si^0 peak (~ 99.6 eV) from substrate and Si-O bond from $HfSiO_x$ (~103.4 eV) are not observed until the sample is etched to the interfacial layer (II), suggesting that the interfacial layer (II) is dominated by $HfSiO_x$. These results indicate that interfacial reactions between the as-deposited HfO_x film and Si substrate occur during the deposition and annealing process. On the other hand, in XPS spectra for Ni1s core level, no binding energy peak is observed in the range of 390-410 eV (see fig.2e). However, it is well known that the binding energy of Ni1s core level for nitrogen atoms (ions) is near 398 eV. This illustrates that there are no nitrogen atoms (ions) present in the film and interface even though the sample has been annealed in N_2 at 300℃for 30 min. Fig. 2f shows the chemical composition of this sample, where one can see that the film (I) is composed of amorphous HfO_x matrix doped with Ge (with content of GeO_x atoms), and the interfacial layer (II) is amorphous $HfSiO_x$ film mixed with Ge atoms. Derived from above XPS depth profile spectra, the statistical analyses on elements in the Ge-doped HfO_x sample are listed in Table 1. The atomic percentage of Ge is about 22 % in the deposited film layer (Ⅰ), while it is 11 % in the interfacial layer (Ⅱ).

As for the reference sample of pure HfO_x film without Ge, its cross-section TEM image (fig.3a) also reveals the existence of a 5 nm-thick amorphous interfacial layer between the 10 nm-thick amorphous film and the Si substrate. Charge-corrected XPS depth profile spectra (fig.3b-3c) confirm that the film is stoichiometric HfO_2 film, while the interfacial layer is $HfSiO_x$. This stacking structure is illustrated by fig.3d.

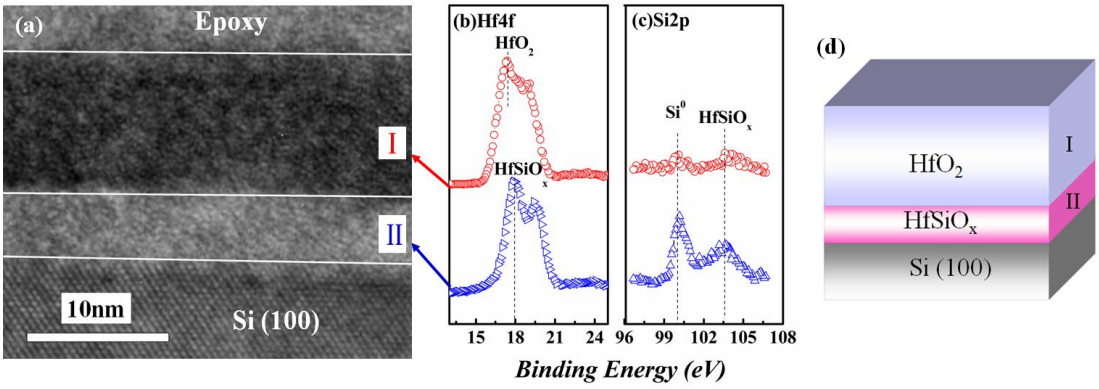

Figure 3 (color online) (a) Cross-section TEM image, XPS depth profile spectra of (b) Hf4f and (c) Si2p core levels, and (d) the composition illustration of the reference sample of pure HfO_x film without Ge.

3.2 Charge storage characteristics of the memory capacitor

Fig. 4 shows high-frequency (1 MHz) C-V curves of the HfO_x films with and without Ge. Both films were measured at room temperature by sweeping the bias voltage from negative to positive and then reverse. The sample of HfO_x shows no hysteresis in the C-V curves (see fig.4a), while the sample of Ge-doped HfO_x film exhibits an obvious anti-clockwise hysteresis, as shown in fig.3b. Moreover, as shown in fig. 4c, the memory window width (the flat band voltage shift $|\Delta V_{FB}|$) is dependent on the amplitude of voltage, i.e., $|\Delta V_{FB}|$ increases with the increase of voltage and reaches the maximum width of 3.15 eV when the voltage increases to 6 V. According to the equation of $N_{ot} = C_{acc} \times |\Delta V_{FB}| / (qA)$ given by Kukli [27], where C_{acc} is the accumulation capacitance, q the electron charge, A the electrode area, and $|\Delta V_{FB}|$ which is 3.15 V corresponds to a trapped charge density (N_{ot}) of 3.5×10^{12} electrons/cm^2. These results demonstrate that the amorphous Ge-doped HfO_x film possesses good charge storage properties. It should be pointed out that $HfSiO_x$ has a bigger band gap (E_g ~ 6.5 eV） than HfO_2 (E_g ~ 5.8 eV) [28], and it is also one of the tunneling/control oxide candidates. Thus, the interfacial layer of $HfSiO_x$ mixed with Ge may act as an additional memory layer, and contribute to the charge storage of the memory cell. However, the interfacial layer degrades the effective permittivity of the whole

sample due to its lower permittivity (ε~11) compared to HfO_2 (ε~25) [28].

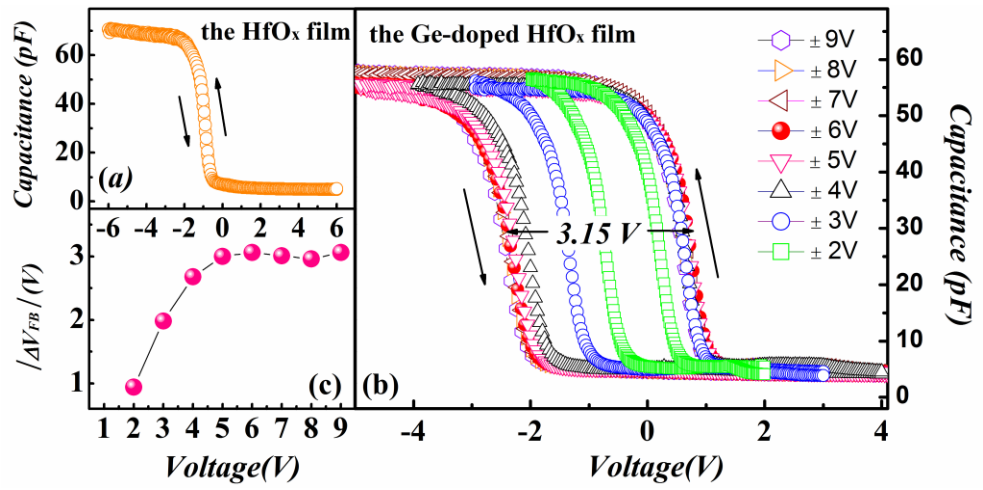

Figure 4 (color online) (a) *C-V* curves of the HfO_x film without Ge, and the voltage-dependence of (b) *C-V* hysteresis and (c) flat band voltage shift ($|\Delta V_{FB}|$) for the Ge-doped HfO_x film.

In order to study the reliability of the memory, the endurance properties of the memory structure are also characterized. After sweeping the bias voltage back and forth between - 6 and 6 V for more than 5×10^4 cycles, the memory window width ($|\Delta V_{FB}|$) has no obvious decrease, while the decrease of accumulation capacitance (C_{acc}) is only less than 10 % (see figs.5a and 5b). This indicates good endurance properties of the memory structure.

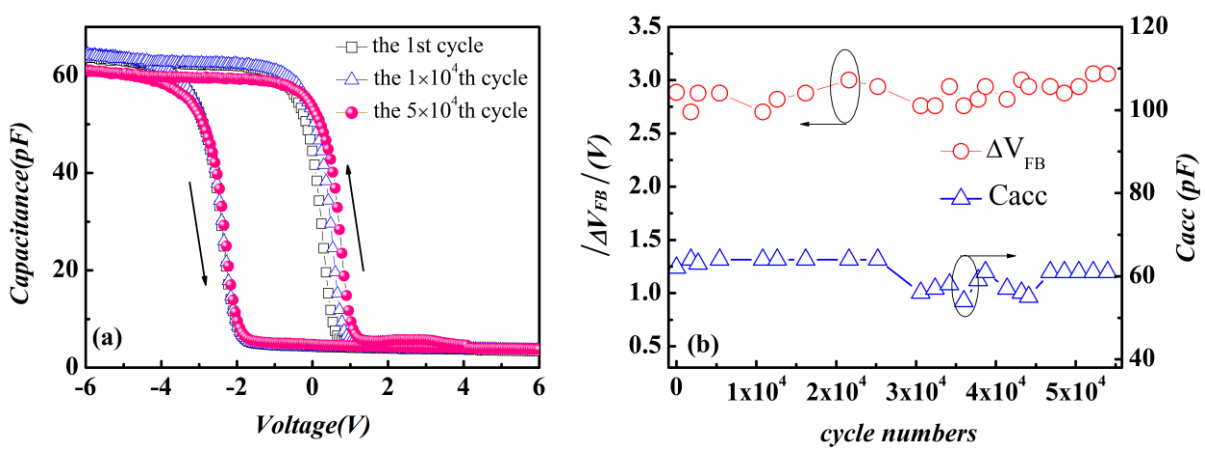

Figure 5 (color online) Stress-time dependence of (a) C-V hysteresis, (b) variations of the flat-band voltage shift ($|\Delta V_{FB}|$) and the accumulation capacitance (C_{acc}) with the sweep cycle numbers for the memory capacitor. The applied bias voltage is swept back and forth between - 6 and 6 V.

3.3 Leakage current characteristic and tunneling mechanism of the memory capacitor

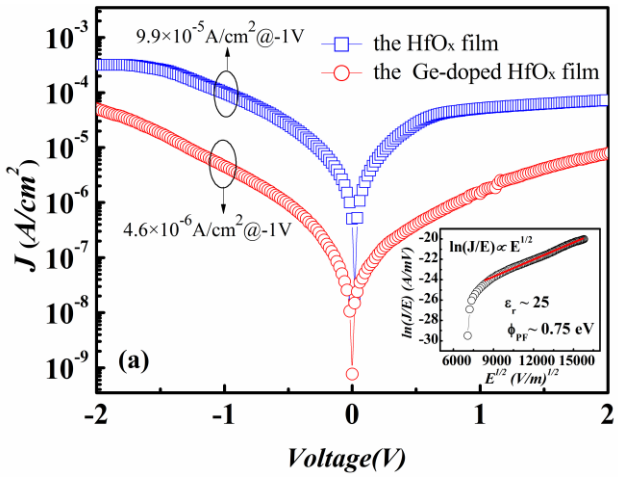

Figure 6 (color online) J-V curves of the HfO_x film with and without Ge. Inset is the J -V plot of the Ge-doped HfO_x film by using the Poole-Frenkel tunneling model ($\ln (J/E) \propto E^{1/2}$). The red straight lines are guides for eye.

As shown in fig.6, the leakage current density (J) of the Ge-doped HfO_x film is 4.6×10^{-6} A/cm^2 at -1V gate voltage which is much smaller than that of the reference HfO_x sample. The possible reason for this phenomenon is that the doped Ge atoms improve the dielectric properties of the HfO_x matrix. Channel-Hot-Electron (CHE) injection [29] is one general tunneling mechanism governing the electron transport in traditional flash memory, but it only works under high electric field (>15 MV/cm). However, the applied electric filed in our sample is only 4-6 MV/cm, so Poole–Frenkel (P–F) tunneling in low electric field is appropriate. Consequently, leakage current density (J) versus gate voltage (V_g) for the memory capacitor is re-plotted by using P-F tunneling model ($\ln (J/E) \propto E^{1/2}$) according to the following equation [30]

$$J_{PF} \propto E \exp\left[\frac{\beta_{PF}\sqrt{E} - q\phi_{PF}}{k_B T}\right]$$

where $\beta_{PF} = \sqrt{\frac{q^3}{\pi\varepsilon_r\varepsilon_0}}$, k_B is the Boltzmann's constant, T is the measurement temperature, q is the elementary charge, and ε_0 is vacuum permittivity. The effective electric filed strength (E) is calculated by using the equation: $E = (V_g - V_{FB})/d$, where V_{FB} is the flat-band voltage, and d is the film thickness. According to the TEM image shown in fig.2a and the C-V curve of the reference HfO_x sample (fig.3a), the Ge-doped HfO_x film thickness is 10 nm, and V_{FB} is about -0.5 V. The permittivity ε_r derived from the slope of the plotted curve is

about 25 which is consistent with the permittivity of stoichiometric HfO_2 film (ε~25) [28]. However, the derived interfacial barrier height (ϕ_{PF}) from the intercept is about 0.75 eV which is lower than the reported value of about 2 eV[31]. The possible reason for the relatively lower band gap of Ge-doped HfO_x film is that the defect levels in the band gap of HfO_x matrix results in the decrease of the valence band offset for Ge/HfO_x interface.

4 Conclusions

A memory capacitor based on amorphous Ge-doped HfO_x film on p-Si (100) substrate has been deposited by means of radio-frequency magnetron sputtering. TEM observation and XPS analyses reveal the partial oxidization of Ge atoms in the amorphous HfO_x matrix and the formation of $HfSiO_x$ interfacial layer. Ge atoms in HfO_x matrix work as memory nodes resulting in a large memory window of 3.15 V, a good endurance property for more than 5×10^4 cycles and a small leakage current density of 4.6×10^{-6}A/cm^2 at -1V gate voltage. These performances are comparable with that of commercial nitride memories, and better than that of many alternative materials, especially in endurance performance. J-V plotting result demonstrates that Poole–Frenkel tunneling is responsible for electron transport in this memory capacitor.

Acknowledgments

This work is supported by the National Natural Science Foundation of China (Grant No. 11274257), the Natural Science Foundation of Chongqing (Grant No. cstc2014jcyjA40029) and the Fundamental Research Funds for the Central Universities of China (Grant Nos. XDJK2014B043 and XDJK2016E123). JYD is grateful to financial support of Hong Kong GRF grant (No. 514512) and Internal Grant from the Hong Kong Polytechnic University (Grant Nos. G-YN42 and G-UA14).

Reference

[1] T.- C. Chang, F.-Y. Jian, S.-Ch. Chen, Y.-T.Tsai, Developments in nanocrystal memory. Materials Today **14**, 608-615 (2011)

[2] M. Mederos, S. N. M. Mestanza, R. Lang, I. Doi, J. A. Diniz, Germanium nanoparticles grown at different deposition times for memory device applications. Thin Solid Films 611, 39-45 (2016)

[3] A. Slav, C. Palade , A. M. Lepadatu, M. L. Ciurea, V. S. Teodorescu, S. Lazanu, A.V. Maraloiu, C. Logofatu , M. Braic , A. Kiss, How morphology determines the charge storage properties of Ge nanocrystals in HfO_2. Scripta Materialia **113**, 135-138(2016)

[4] S. Das, S. Manna, R. Singha, A. Anopchenko, N. Daldosso, L. Pavesi, A. Dhar, S. K. Ray, Light emission and floating gate memory characteristics of germanium nanocrystals. Phys. Status Solidi A **208**, 635–638 (2011)

[5] S.-W. Ryu, Y.- K. Choi, C. B. Mo, S. H. Hong, P. K. Park, S.-W .Kang, A thickness modulation effect of HfO_2 interfacial layer between double-stacked Ag nanocrystal for nonvolatile memory device applications. J. Appl. Phys.**101**,026109 (2007)

[6] L. Khomenkova, B. S Sahu, A. Slaoui, F. Gourbilleau, Hf-based high-k materials for Si nanocrystal floating gate memories, Nanoscale Res. Lett. **6**,172(2011)

[7] S. Wang, J. Pu, D. S. H. Chan, B. J. Cho, K. P. Loh, Wide memory window in graphene oxide charge storage nodes, Appl. Phys. Lett. **96**, 143109 (2010).

[8] X. Y. Qiu, G. D. Zhou, J. Li, Y. Chen, X. H. Wang , J. Y. Dai , Memory characteristics and tunneling mechanism of Ag nanocrystal embedded $HfAlO_x$ films on $Si_{83}Ge_{17}$/Si substrate , Thin Solid Films **562**, 674-679 (2014)

[9] K. C. Chan, P. F. Lee, J. Y. Dai, Single electron tunneling and Coulomb blockade effect in HfAlO/Au nanocrystals/ HfAlO trilayer nonvolatile memory structure. Appl. Phys. Lett. **92**, 143117 (2008)

[10] P. F. Lee, X. B. Lu, J. Y. Dai, H. L. W. Chan, E. Jelenkovic , K. Y. Tong, Memory effect and retention property of Ge nanocrystal embedded Hf-aluminate high-k gate dielectric. Nanotechnology **17**, 1202-1206 (2006).

[11] X. B. Lu, P. F. Lee, J. Y. Dai, Synthesis and memory effect study of Ge nanocrystals embedded in $LaAlO_3$ high-kdielectrics. Appl. Phys. Lett. **86**, 203111(2005)

[12] W. R. Chen, T. C. Chang, Y. T. Hsieh, C. Y. Chang, Formation and nonvolatile memory application of Ge nanocrystals by using internal competition reaction of $Si_{1.33}Ge_{0.67}O_2$ and $Si_{2.67}Ge_{1.33}N_2$ layers. IEEE Trans. on Nanotechnology **8,**185-189 (2009).

[13]Y.-C. King, T. J. King, C. Hu, Charge-trap memory device fabricated by oxidation of $Si_{1-x}Ge_x$. IEEE Trans. on Electro. Devices **48**, 696-700 (2001)

[14] R. C. Jeff, Jr. M. Yun, B. Ramalingam, B. Lee, V. Misra, G. Triplett, S. Gangopadhyay, Charge storage characteristics of ultra-small Pt nanoparticle embedded GaAs based non-volatile memory. Appl. Phys. Lett. **99**, 072104 (2011)

[15] D.-W. Kim, F. E. Prins, T. Kim, S. Hwang, C. H. Lee, D.-L. Kwong, S. K. Banerjee, Reduction of charge-transport characteristics of SiGe dot floating gate memory device with ZrO_2 tunneling oxide. IEEE Trans. on Electro. Devices **50**, 510 -513 (2003)

[16] S.-T. Han, Y. Zhou , C. D. Wang , L. F. He, W. J. Zhang, V. A. L. Roy, Layer-by-layer-assembled reduced graphene oxide/gold nanoparticle hybrid double-floating-gate structure for low-voltage flexible flash memory. Adv. Mater.**25**, 872–877 (2013)

[17] M. J. Kang , K.-J. Baeg , D.Y. Khim, Y.-Y. Noh , D.-Y. Kim, Organic nano-floating-gate memory: effects of metal nanoparticles and blocking dielectrics on memory characteristics. Adv. Funct. Mater. 23, 3503–3512 (2013)

[18] X. Gao, Ch.-H. Liu, X.-J. She, Q.-L. Li, J. Liu, S.-D. Wang, Photon-energy-dependent light effects in organic nano-floating-gate nonvolatile memories. Organic Electronics **15,** 2486–2491 (2014)

[19] Y. Mei, C. Zhanga, Z. V. Vardenya , O. D. Jurchescua, Electrostatic gating of hybrid halide perovskite field-effect transistors: balanced ambipolar transport at room-temperature. MRS Communications **5**, 297-301 (2015)

[20] H. Wang, Y. Wang, J. Feng, C. Ye, B. Y. Wang, H. B. Wang, Q. Li, Y. Jiang, A. P. Huang, Z. S. Xiao, Structure and electrical properties of HfO_2 high-k films prepared by pulsed laser deposition on Si (100). Appl. Phys. A **93**, 681-684 (2008)

[21] M. N. Jones, Y. W. Kwon, D. P. Norton, Dielectric constant and current transport for HfO_2 thin films on ITO. Appl. Phys. A **81**, 285–288 (2005)

[22] Y.-H. Lin, Ch.-H. Chien, Ch.-T. Lin, Ch.-Y. Chang, T.-F. Lei, High-performance nonvolatile HfO_2 nanocrystal memory. IEEE Electro. Device Lett. **26**, 154-156 (2005)

[23] S. Choi, S-S. Kim, M. Chang, H. Hwang, S. Jeon, Ch. Kim, Highly thermally stable TiN nanocrystals as charge trapping sites for nonvolatile memory device applications. Appl. Phys. Lett. **86**, 123110(2005)

[24] Sh.-M. Yang, Ch.-H. Chien, J.-J. Huang, T.-F. Le, Nonvolatile flash memory devices using CeO_2 nanocrystal trapping layer for two-bit per cell applications. Jap. J. Appl. Phys. **46**, 3291-3295 (2007)

[25] J. D. Cox, D. D. Wagman, V. A. Medvedev. CODATA Key Values for Thermodynamics.(New York: Hemisphere Publishing Corp,1989),pp. 271

[26] D. R. Lide, CRC Handbook of Chemistry and Physics. 90th edn.(Boca Raton, FL: CRC Press Inc, 2009),pp. 5-12–5-17

[27] K. Kukli, M. Ritala, T. Sajavaara, J. Keinonen, M. Leskelä, Comparison of hafnium oxide films grown by atomic layer deposition from iodide and chloride precursors. Thin Solid Films **416,** 72-79 (2002)

[28]A. P. Huang, Z. C. Yang, Paul K. Chu, Hafnium-based High-k Gate Dielectrics, in Advances in Solid State

Circuits Technologies, ed By Paul K. Chu (InTech,2010),p. 333-350

[29] B. Eitan, D. Frohman, Hot-electron injection into the oxide in n-channel MOS devices. IEEE Trans. on Electro. Devices **28**, 328–340 (1981)

[30] P. Rottla ̈nder, M. Hehn, A. Schuhl, Determining the interfacial barrier height and its relation to tunnel magnetoresistance. Phys. Rev. B **65**, 054422 (2002)

[31] V. V. Afanas'ev, A. Stesmans, Energy band alignment at the (100)Ge/HfO_2 interface. Appl. Phys. Lett. 84 2319-2321(2004)